Safety-aware trajectory scaling for human-robot collaboration with prediction of human occupancy

Matteo Ragaglia, Andrea Maria Zanchettin and Paolo Rocco

Abstract— **Planning and control of an industrial manipulator for safe Human-Robot Collaboration (HRC) is a difficult task because of two conflicting requirements: ensuring the worker's safety and completing the task assigned to the robot. This paper proposes a trajectory scaling algorithm for safe HRC that relies on real-time prediction of human occupancy. Knowing the space that the human will occupy within the robot stopping time, the controller can scale the manipulator's velocity allowing safe HRC and avoiding task interruption. Finally, experimental results are presented and discussed.**

I. Introduction

Nowadays industrial robots are able to offer fast and accurate task execution in various industrial applications (welding, painting, palletizing, ecc.), but they are still rarely or inefficiently used within Small and Medium-sized Enterprises (SMEs), mainly because of some well-known issues. Installation, setup and programming of a robotized workstation are time-consuming activities that require a lot of skilled engineering effort. Moreover for safety reasons workstations need to be separated from the human workspace by physical barriers (see [1]).

For SMEs, characterized by limited budgets and by constraints on space consumption, the massive use of industrial robots is still not properly affordable. In order to overcome these limitations physical barriers separating the robot and the human workspaces must be removed, but this lack of artificially imposed safety must be compensated for by guaranteeing that Human-Robot Collaboration (HRC) is both safe and efficient: the human worker should not be harmed by the robot (see [2], [3]), but also production constraints (i.e. pre-programmed execution paths) should not be violated, in order to preserve the manipulator's productivity.

Recently several contributions to the problem of planning and control of industrial manipulators for safe HRC have been proposed. In the field of collision avoidance, [4] presents an approach based on avoidance maneuvers. [5] describes a passivity based controller for safe human-robot coexistence that produces slower motion profiles when the human/robot distance decreases. Another collision avoidance strategy based on evasive motion is presented in [6]. Clearly, the main limitation of these approaches consists in their incompatibility with constraints on the manipulator's trajectory imposed by the task.

On the other hand, as far as collision detection (see [7]) and reaction are concerned, [8] presents different collision reaction strategies aiming at ensuring safety to the human during physical interaction, while [9] proposes a real-time self collision detection algorithm for both humanoid and industrial robots based on swept volumes.

When it comes to prescriptions imposed by safety standards, the most recent ones, like for instance [10], [11] and [12], establish speed and separation monitoring criteria according to which a minimum separation distance (depending on Tool Center Point velocity and/or payload) must be maintained between an industrial manipulator and a human worker. Control policies that are compliant with these standards have been presented in [13] and [14].

To improve the effectiveness of these policies it is necessary to predict "human occupancy", i.e. the space occupied by the human during the next T_s seconds. In the last few years several works have focused on human motion and occupancy prediction. [15] presents a strategy for predicting in real time the trajectory of a human worker walking inside a robotic cell, while [16] describes vision-based safety-oriented control strategies that rely on a conservative prediction of human workers' occupancy. Finally a technique for predicting the human workspace occupancy on the basis of learned human motion trajectories is presented is [17].

The main contribution of this work to the field of HRC consists in extending the safety measure presented in [14] in order to account for more complex obstacles, like for instance moving human workers inside the robotic cell. First, the safety requirements are extended for the case of arbitrary shaped convex obstacles and unions of such convex polytopes. Then, a simple kinematic model of the human being is introduced in order to predict human occupancy in terms of a series of swept volumes, that are convex polytopes indeed.

Considering time T_s equal to the robot braking time, or stopping time (see [18]), we obtain the human occupancy by the time the manipulator completely stops. Consequently it is possible to develop a trajectory scaling strategy that adapts the robot's speed in a conservative way with respect to the predicted human occupancy. As a result we are able to guarantee safe HRC without violating the pre-programmed robot path.

The remainder of this work is organized as follows. Section II summarizes our previous work regarding safety

The authors are with Politecnico di Milano, Dipartimento di Elettronica, Informazione e Bioingegneria, Piazza L. Da Vinci 32, 20133, Milano, Italy (email: matteo.ragaglia@polimi.it, andreamaria.zanchettin@polimi.it, paolo.rocco@polimi.it). The accompanying video is also available at: http://www.youtube.com/watch?v=Z7DgzHC9e9E

978-1-4673-7509-2/15/$31.00

constraints. In Section III these constraints are extended considering arbitrarily shaped convex obstacles. The prediction of human occupancy and its formalization as a series of convex obstacles is detailed in Section IV, while Section V focuses on human occupancy-based trajectory generation. Finally, Section VI presents the case study against which our proposed method has been experimentally tested and validated.

II. Background on safety constraints

We here report some background material on the derivation of safety constraints for a point obstacle as introduced in [14]. Consider Fig. 1 which represents a point obstacle $\boldsymbol{r_{obst}}$ as well as a generic robotic link, whose endpoints are at positions $\boldsymbol{r_a}$ and $\boldsymbol{r_b}$. At all time, the robot trajectory must

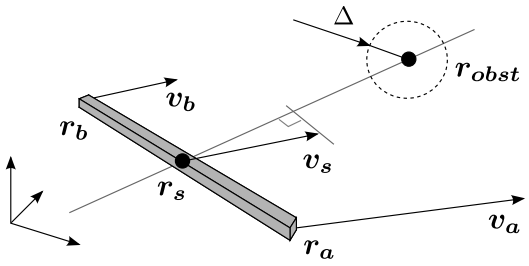

Fig. 1. A rigid beam representing one link

obey the following safety requirement

$$\text{velocity} \cdot T_s \leq \max\left(0, \text{distance} - \text{clearance}\right)$$

where the braking time T_s possibly depends on the robot payload [1] and the clearance parameter allows to take into account both link and obstacle dimensions. In order to relate such a safety requirement, we introduce the following inequality constraint valid for a generic point $\boldsymbol{r_s}$ on the robot link, with velocity $\boldsymbol{v_s}$

$$\boldsymbol{v_s}^T \frac{\boldsymbol{r_{obst}} - \boldsymbol{r_s}}{\|\boldsymbol{r_{obst}} - \boldsymbol{r_s}\|} T_s \leq \max\left(0, \|\boldsymbol{r_{obst}} - \boldsymbol{r_s}\| - \Delta\right) \quad (1)$$

where Δ is a clearance parameter. This constraint can be further arranged as

$$\begin{aligned} \boldsymbol{v_s}^T \left(\boldsymbol{r_{obst}} - \boldsymbol{r_s}\right) T_s \leq \\ \max\left(0, \|\boldsymbol{r_{obst}} - \boldsymbol{r_s}\|^2 - \Delta \|\boldsymbol{r_{obst}} - \boldsymbol{r_s}\|\right) \end{aligned} \quad (2)$$

Assume now the following parameterization of the link in terms of positions and velocities of its end points

$$\boldsymbol{r_s} = \boldsymbol{r_a} + s\left(\boldsymbol{r_b} - \boldsymbol{r_a}\right) \quad \boldsymbol{v_s} = \boldsymbol{v_a} + s\left(\boldsymbol{v_b} - \boldsymbol{v_a}\right) \quad (3)$$

In order enforce the safety constraints, we require the inequality in (2) to be satisfied for all $s \in [0, 1]$. The left hand side becomes

$$\begin{aligned} \boldsymbol{v_s}^T \left(\boldsymbol{r_{obst}} - \boldsymbol{r_s}\right) = \boldsymbol{v_a}^T \left(\boldsymbol{r_{obst}} - \boldsymbol{r_a}\right) \\ + s\left(\boldsymbol{v_b} - \boldsymbol{v_a}\right)^T \left(\boldsymbol{r_{obst}} - \boldsymbol{r_a}\right) \\ - s\boldsymbol{v_a}^T \left(\boldsymbol{r_b} - \boldsymbol{r_a}\right) \\ - s^2 \underbrace{\left(\boldsymbol{v_b} - \boldsymbol{v_a}\right)^T \left(\boldsymbol{r_b} - \boldsymbol{r_a}\right)}_{=0} \end{aligned} \quad (4)$$

As for the right hand side, notice that

$$\begin{aligned} \left[\max\left(0, \ \|\boldsymbol{r_{obst}} - \boldsymbol{r_s}\| - \Delta\right)\right]^2 \leq \\ \max\left(0, \ \|\boldsymbol{r_{obst}} - \boldsymbol{r_s}\|^2 - \Delta \|\boldsymbol{r_{obst}} - \boldsymbol{r_s}\|\right) \end{aligned} \quad (5)$$

As a result, the set of inequalities describing the safety constraints can be written as follows

$$\alpha + \beta s \leq g\left(s\right), \forall s \in [0, 1] \quad (6)$$

where

$$\begin{aligned} \alpha &= T_s \boldsymbol{v_a}^T \left(\boldsymbol{r_{obst}} - \boldsymbol{r_a}\right) \\ \beta &= T_s \left(\boldsymbol{v_b} - \boldsymbol{v_a}\right)^T \left(\boldsymbol{r_{obst}} - \boldsymbol{r_a}\right) - T_s \boldsymbol{v_a}^T \left(\boldsymbol{r_b} - \boldsymbol{r_a}\right) \\ g\left(s\right) &= \left[\max\left(0, \ \|\boldsymbol{r_{obst}} - \boldsymbol{r_s}\| - \Delta\right)\right]^2 \end{aligned} \quad (7)$$

By noticing that the left hand side is a linear function in s it is possible to write the following sufficient condition for the safety constraint (6) to be satisfied

$$\max\left\{\alpha, \alpha + \beta\right\} \leq \min_s g\left(s\right) \quad (8)$$

In turn, within the right hand side term, it is possible to exchange the $\min$ and $\max$ operators yielding

$$\min_s g\left(s\right) = \left[\max\left(0, \ \min_s \|\boldsymbol{r_{obst}} - \boldsymbol{r_s}\| - \Delta\right)\right]^2 \quad (9)$$

where the term $\min_s \|\boldsymbol{r_{obst}} - \boldsymbol{r_s}\| - \Delta$ represents, when it is positive, the distance between a sphere of radius Δ centered in $\boldsymbol{r_{obst}}$ and the segment from $\boldsymbol{r_a}$ to $\boldsymbol{r_b}$. Finally, we obtain the following couple of inequalities

$$\begin{aligned} \alpha = T_s \left(\boldsymbol{r_{obst}} - \boldsymbol{r_a}\right)^T \boldsymbol{v_a} \leq \min_s g\left(s\right) \\ \alpha + \beta = T_s \left(\boldsymbol{r_{obst}} - \boldsymbol{r_a}\right)^T \boldsymbol{v_b} \\ - T_s \left(\boldsymbol{r_b} - \boldsymbol{r_a}\right)^T \boldsymbol{v_a} \leq \min_s g\left(s\right) \end{aligned} \quad (10)$$

Summarizing, the minimum separation distance criterion can be written in matrix form as $T_s \boldsymbol{E}\dot{\boldsymbol{q}} \leq \boldsymbol{f}$ where

$$\begin{aligned} \boldsymbol{E} &= \begin{bmatrix} \left(\boldsymbol{r_{obst}} - \boldsymbol{r_a}\right)^T \boldsymbol{J_a} \\ \left(\boldsymbol{r_{obst}} - \boldsymbol{r_a}\right)^T \boldsymbol{J_b} - \left(\boldsymbol{r_b} - \boldsymbol{r_a}\right)^T \boldsymbol{J_a} \end{bmatrix} \\ \boldsymbol{f} &= \min_s g\left(s\right) \begin{bmatrix} 1 \\ 1 \end{bmatrix} \end{aligned} \quad (11)$$

$\boldsymbol{J_a}$ and $\boldsymbol{J_b}$ are position Jacobians of the two link end points.

III. Extension to arbitrary shaped convex obstacles

So far, the safety requirement has been expressed for fixed point obstacles. We here extend the safety constraints to the case of obstacles having more complex geometry. A further extension dealing with moving obstacles, and particularly dealing with human workers, will be discussed in the next Section.

Consider a generic polytopic obstacle $\mathcal{O}$ as shown in Fig. 3. The constraints to be enforced for such an obstacle can be written as follows

$$T_s \boldsymbol{E}\left(\boldsymbol{r_{obst}}\right) \dot{\boldsymbol{q}} \leq \boldsymbol{f}\left(\boldsymbol{r_{obst}}\right), \forall \boldsymbol{r_{obst}} \in \mathcal{O} \quad (12)$$

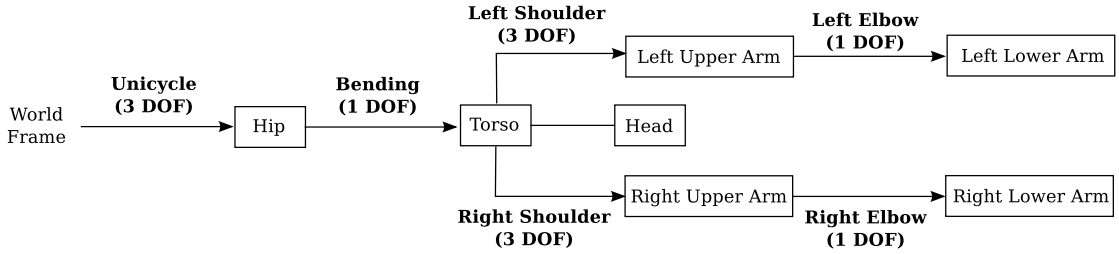

Fig. 2. Kinematic model of the human: DOFs, frames and bodies

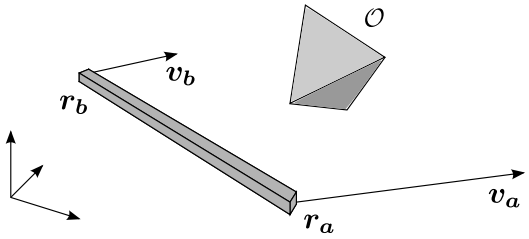

Fig. 3. A generic polytopic (convex) obstacle

The number of constraints to be enforced at run time is conceptually infinite, i.e. one per each point belonging to $\mathcal{O}$. However, some geometrical properties of the obstacle can be exploited in order to make the problem tractable.
A sufficient condition for (12) to be satisfied for all points $\boldsymbol{r_{obst}} \in \mathcal{O}$ is

$$T_s \boldsymbol{E}\left(\boldsymbol{r_{obst}}\right) \dot{\boldsymbol{q}} \leq d \begin{bmatrix} 1 \\ 1 \end{bmatrix}, \forall \boldsymbol{r_{obst}} \in \mathcal{O} \tag{13}$$

where the right hand side term $d = \min_{\boldsymbol{r_{obst}} \in \mathcal{O}} \left\| \boldsymbol{f}\left(\boldsymbol{r_{obst}}\right) \right\|_\infty$ represents the minimum distance between the link of the robot and the polytopic obstacle $\mathcal{O}$ and can be easily computed using the GJK algorithm, [19]. Moreover, notice that the left hand side term is linear with respect to the parameter $\boldsymbol{r_{obst}} \in \mathcal{O}$. Therefore the safety constraints regarding the pair link-obstacle can be written as follows

$$T_s \left(\boldsymbol{r_{obst}}^T \boldsymbol{E_0} + \boldsymbol{E_1} \right) \dot{\boldsymbol{q}} \leq d, \forall \boldsymbol{r_{obst}} \in \mathcal{O} \tag{14}$$

For linearity (and thus convexity) the aforementioned constraint (which actually consists of an infinite number of scalar inequalities) can be equivalently written in terms of the vertices (thus a limited number) of the polytope representing the obstacle $\mathcal{O}$, hence $\forall \boldsymbol{r_{obst}} \in vert\left(\mathcal{O}\right)$.

IV. Prediction of Human Occupancy

In the previous Sections, we presented a mathematical formulation to represent the safety constraint arising in a typical human-robot collaboration scenario. As already discussed, despite the possibility to consider arbitrarily geometrically shaped obstacles, their motion is not directly accounted for in the expression of the safety requirement.
In a HRC setup, the motion of the human, and particularly the prediction of his/her occupancy, has to be clearly taken into account to safely adjust the trajectory of the robot. In order to predict the motion of the human, we make use of a relatively simple kinematic model suitable for real-time calculations. The model of the human, see Fig. 2, consists of one lumped one-DOF (flexion/extension) torso, a head (fixed), two four-DOF arms and a mobile base to represent the walking kinematics. The main objective of this Section is to introduce a simple algorithm that predicts a strictly conservative area around the human silhouette, which can be possibly reached in T_s seconds, i.e. within the time needed by the robot to brake or stop.
In the following further details of the kinematic model of the human arm, as well as on the kinematics of walking, are given. The predicted reachable area will be represented in terms of superposition of each possible motion (swept motion) in the corresponding prediction horizon.

A. Modelling the human arm kinematics

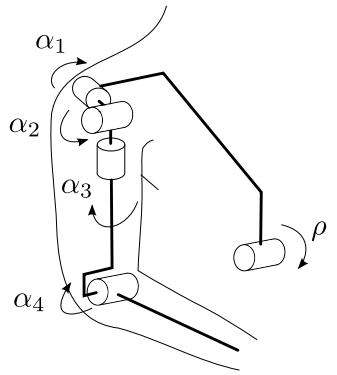

Fig. 4. Kinematic model of the human (right) arm and torso flexion/extension angle ρ.

As for the human arm, we make use of a well-known model, sketched in Fig. 4, comprising one spherical joint representing the shoulder and one additional degree of freedom for the elbow, see e.g. [20], [21]. The workspace of the human arm is clearly limited due to some intrinsic limitations in the gleno-humeral joint (shoulder) as well as in the elbow. Differently from robots, however, these limits are coupled, as described e.g. in [22]. In particular, the range of motion of the human arm is limited to the region identified by the following constraints[1]

$$-9 \leq \alpha_1 \leq 160 \tag{15a}$$

[1]All listed parameters are in degrees.

$$-43+\frac{\alpha_1}{3}\leq\alpha_2\leq 153-\frac{\alpha_1}{6} \tag{15b}$$

$$-90+\frac{7\alpha_1}{9}-\frac{\alpha_2}{9}+\frac{2\alpha_1\alpha_2}{810}\leq\alpha_3\leq 60+\frac{4\alpha_1}{9}-\frac{5\alpha_2}{9}+\frac{5\alpha_1\alpha_2}{810} \tag{15c}$$

$$20\leq\alpha_4\leq 180 \tag{15d}$$

where $\alpha_1,\ldots,\alpha_4$ are the arm joint angles shown in Figure 4. As for the flexion/extension of the torso we considered the following bound

$$-30\leq\rho\leq 90 \tag{16}$$

where ρ is the torso bending angle shown again in Figure 4. Finally, as all joint limits characterizing the human upper body are in place, from a given arm/torso configuration, i.e. ρ and $\boldsymbol{\alpha}$, and the corresponding maximum allowed velocities $\dot{\rho}^{max}$ and $\dot{\boldsymbol{\alpha}}^{max}$, it is quite simple to compute the reachable set in T_s seconds by simply computing

$$\boldsymbol{\alpha_{T_s}}=\boldsymbol{\alpha}\pm T_s\dot{\boldsymbol{\alpha}}^{\boldsymbol{max}}\quad \rho_{T_s}=\rho\pm T_s\dot{\rho}^{max} \tag{17}$$

and limiting the result to the region inside the joint limits, previously introduced in (15).

B. Modelling the human walk kinematics

For the description of the kinematics of walking, as suggested in e.g. [15], [23], we make use of the unicycle model

$$\dot{x}=v\cos\theta\quad\dot{y}=v\sin\theta\quad\dot{\theta}=\omega \tag{18}$$

together with the following constraints on its inputs

$$0\leq v\leq v^{max}\quad|\omega|\leq\omega^{max} \tag{19}$$

where x, y and θ describe the walking human pose with respect to the world base frame, v is the linear velocity and ω is the angular velocity.

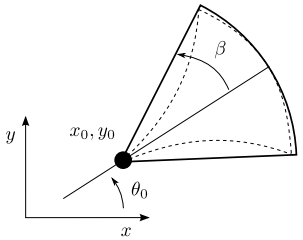

Fig. 5. Unicycle reachable set (dashed) and its convex approximation (solid bold)

Similarly with the previous case, we here aim at computing the reachable set in T_s seconds. For this, we consider every possible combination of inputs. In particular, for the case $v(t)=v^{max}$, $\omega(t)=0$, the solution of (18) after T_s seconds is as follows

$$\begin{aligned}x_{T_s}&=x_0+v^{max}T_s\cos\theta_0\\ y_{T_s}&=y_0+v^{max}T_s\sin\theta_0\\ \theta_{T_s}&=\theta_0\end{aligned} \tag{20}$$

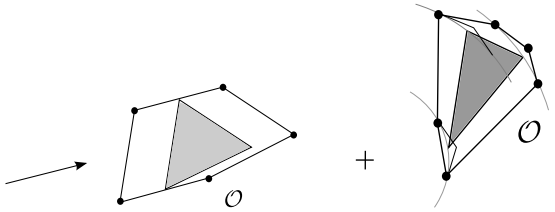

(a) Translational (b) Rotational

Fig. 6. Swept volume of convex objects

while similarly for $v(t)=v^{max},\omega(t)=\pm\omega^{max}$

$$\begin{aligned}x_{T_s}&=x_0\pm\frac{v^{max}}{\omega^{max}}\left[\sin\left(\theta_0\pm\omega^{max}T_s\right)-\sin\theta_0\right]\\ y_{T_s}&=y_0\mp\frac{v^{max}}{\omega^{max}}\left[\cos\left(\theta_0\pm\omega^{max}T_s\right)-\cos\theta_0\right]\\ \theta_{T_s}&=\theta_0\pm T_s\omega^{max}\end{aligned} \tag{21}$$

The reachable set of the unicycle can be conservatively represented by a circular sector of radius $R=v^{max}T_s$, spanning an angle

$$\beta=2\cos^{-1}\left(\frac{\sin\left(\omega^{max}T_s\right)}{\sqrt{2-2\cos\left(\omega^{max}T_s\right)}}\right)$$

symmetrically with respect to the current direction of motion θ_0, see Fig. 5. This way the human walking model can be described as a composition of two independent degrees of freedom: a rotational one followed by a translational one. The corresponding reachable set follows immediately from this approximation.

C. Prediction and representation of the human occupancy

In the following we present a method to predict the occupancy of the human silhouette in terms of a series of convex polytopes, using the computation of the reachable sets for each degree of freedom.

Assume a given configuration of the human upper body, say

$$\boldsymbol{p}=\begin{bmatrix}x & y & \theta & \rho & \boldsymbol{\alpha^{right}} & \boldsymbol{\alpha^{left}}\end{bmatrix}^T \tag{22}$$

where $\boldsymbol{\alpha^{right}}$ and $\boldsymbol{\alpha^{left}}$ are respectively the joint angles vectors for the right arm and for the left arm.

First, for each DOF, the corresponding reachable set is computed as before, obtaining the maximum range of motion in T_s seconds

$$\boldsymbol{p_{inf}}\leq\boldsymbol{p}\leq\boldsymbol{p^{sup}} \tag{23}$$

where $\boldsymbol{p_{inf}}$ and $\boldsymbol{p^{sup}}$ can be computed at first as $\boldsymbol{p}\pm T_s\dot{\boldsymbol{p}}^{\boldsymbol{max}}$ and applying saturations with respect to joint limits at a later stage.

The problem of computing and representing the human occupancy is now to map the inequalities in (23) into a corresponding occupancy in the 3D Cartesian space.

Assume a convex object $\mathcal{O}$ representing a human limb (head, thorax, left and right arm) is given by means of its vertices set. Then, referring to the tree describing the human kinematic model in Fig. 2, a list of degrees of freedom from the current limb to the world frame can be

arranged. For a prismatic joint the corresponding translation is applied to each point of the convex hull representing $\mathcal{O}$. The translational swept volume of $\mathcal{O}$ is then obtained by computing the convex hull of the resulting points, see Fig. 6(a). In turn, for a rotational degree of freedom, we exploit one of the method described in [9]. In particular, for each point of $\mathcal{O}$, an arc is constructed and approximated by a triangle. The rotational swept volume of $\mathcal{O}$ can be easily obtained as the convex hull of the vertices of all the triangles, see Fig. 6(b).

This procedure is then iteratively applied for each degree of freedom from the limb to the world frame and for each limb composing the kinematic model of the human. The resulting representation of human occupancy is shown in Fig. 7.

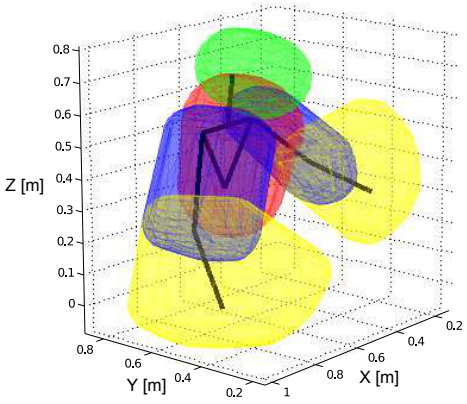

Fig. 7. Representation of the human occupancy prediction. The swept volumes corresponding to each limb are highlighted with different colours.

V. Safety-aware Trajectory Generation Algorithm

This Section describes an efficient algorithm to solve the safety-aware trajectory motion planning problem by suitably scaling a pre-planned trajectory in time. The compatibility of the trajectory scaling technique with respect to a closed-ended industrial controller is also discussed. Assume the following well-known parametrization of the task with respect to time:

$$\boldsymbol{x}(\tau) \quad \boldsymbol{x}'(\tau) = \frac{\partial \boldsymbol{x}}{\partial \tau} \tag{24}$$

where τ is the time variable and $\boldsymbol{x}(\cdot)$ is a differentiable task function specifying the desired trajectory. Let $\delta \in [0, 1]$ be a scalar quantity adopted to kinematically scale the trajectory in time. The value $\delta = 1$ corresponds to the nominal trajectory, i.e. executed at programmed speed, while $\delta = 0$ forces the robot to stop. Similarly to the concept originally developed in [8], we introduce the following Linear Programming (LP) optimization problem:

$$\max_{\delta} \delta \tag{25a}$$

$$T_s \boldsymbol{E}(\boldsymbol{r_{obst}}) \dot{\boldsymbol{q}} \delta \leq d \begin{bmatrix} 1 \\ 1 \end{bmatrix}, \forall \boldsymbol{r_{obst}} \in \mathcal{O} \tag{25b}$$

$$0 \leq \delta \leq 1 \tag{25c}$$

This way, the solution of the LP problem tends to maximize the throughput of the robot, while being consistent with the safety requirement, thus resulting in a trade-off between safety and productivity. Each pair link-obstacle is accounted for in the inequality constraints (25b) which can also consider, by selecting a suitable clearance parameter Δ, the size of each link as well as an actual clearance parameter. Notice that the problem always has a trivial solution $\delta = 0$, which guarantees its solvability in realistic applications. Finally, to avoid chattering behaviour of variable δ that would result in multiple activations and suspensions of the task, a hysteresis has been implemented: once δ is set to zero, the output of the trajectory scaling algorithm is forced to zero, until the minimum distance exceeds a predefined threshold.

VI. An Experimental Case Study

In this Section we describe a relevant case study and we present the result obtained by applying our proposed approach. The robot has to accomplish a simple pick and place task while cooperating with the human worker by scaling the Tool Center Point velocity without disrupting the pre-programmed path.

A. Experimental Setup

The experimental setup is shown in Fig. 8. It consists of:

- ABB IRB 140 robot: a 6 axes industrial robot with 6 kg maximum payload. Its position controlled by an industrial ABB IRC 5 controller and programmed through the proprietary RAPID language. RAPID instructions allow to specify the programmed speed along the given path (see again [14]);
- Microsoft Kinect: a RGBD motion sensing camera developed by Microsoft. Kinect is used to detect the presence of a human worker and it allows to determine his/hers kinematic configuration with respect to the model described in Section IV;
- External PC: a real-time PC that computes the human swept volumes and evaluates the kinematic scaling parameter δ according to the distance between the swept volumes and the manipulator. The feedback to the IRC5 robot controller has been implemented with standard TCP/IP sockets.

Fig. 8. Experimental setup

B. Experimental Validation

In order to validate our trajectory scaling strategy the robot has been assigned a typical pick and place task consisting in picking the compact discs stored in the CD rack and releasing them into a green box. During task execution a human worker approaches the manipulator in order to substitute the green box containing the CDs released by the robot with an empty one (see again Figure 8).

Figure 9 clearly demonstrates the effectiveness of our approach. If the predicted human occupancy is far away from the manipulator the kinematic scaling parameter δ is equal to 1 and the robot executes the nominal trajectory. Whenever the human worker approaches the robot, the distance between its predicted occupancy and the manipulator rapidly decreases and consequently δ is lowered until it reaches zero. Once again Figure 9 shows that when the kinematic scaling parameter is equal to zero the manipulator completely stops allowing the human worker to safely interact with it (i.e. by substituting the green box). As mentioned before, δ is set back to 1 and the robot resumes the nominal trajectory as soon as the distance between the predicted human occupancy and the robot overcomes the predefined threshold. The attached video integrates the experiment description.

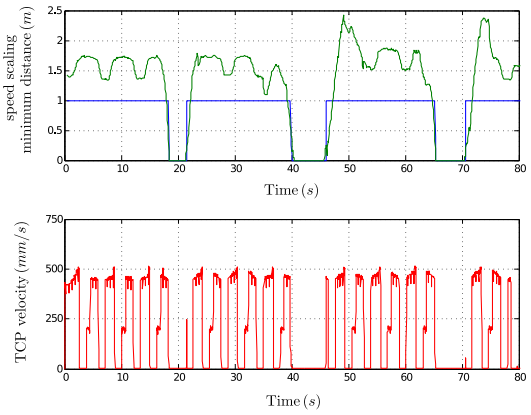

Fig. 9. Validation Experiment: the first plot represents speed scaling (solid blue) and minimum distance (solid green), while the second plot shows robot Tool Center Point velocity (solid red).

VII. Conclusions

This paper discusses an approach to trajectory scaling for safe HRC. The proposed solution relies on real-time evaluation of human occupancy that allows to safely scale the manipulator's velocity. Safer man-machine collaboration, while maintaining path constraints, is achieved. Details on the actual implementation of the proposed approach are discussed and experimental results are presented. The main future developments are represented by the possibility to consider more complex motion models for the human being accounting for velocity and acceleration of the body joints.

References

[1] *ANSI/RIA R15 06 1999 "Safety requirements for industrial robots and robot systems"*.

[2] S. Haddadin, A. Albu-Schaeffer, and G. Hirzinger, "Requirements for safe robots: measurements, analysis and new insights," *International Journal of Robotics Research*, vol. 28, pp. 1507–1527, 2008.

[3] S. Haddadin, S. Haddadin, A. Khoury, T. Rokahr, S. Parusel, R. Burgkart, A. Bicchi, and A. Albu-Schaeffer, "On making robots understand safety: Embedding injury knowledge into control," pp. 1578–1602, 2012.

[4] P. Fiorini and Z. Shiller, "Motion planning in dynamic environments using velocity obstacles," *International Journal of Robotics Research*, vol. 17, no. 7, pp. 760–772, 1998.

[5] A. M. Zanchettin, B. Lacevic, and P. Rocco, "A novel passivity-based control law for safe human-robot coexistence," in *Intelligent Robots and Systems (IROS), 2012 IEEE/RSJ International Conference on*, 2012.

[6] B. Lacevic, P. Rocco, and A. M. Zanchettin, "Safety assessment and control of robotic manipulators using danger field," *Robotics, IEEE Transactions on*, vol. 29, pp. 1257–1270, 2013.

[7] P. Jiménez, F. Thomas, and C. Torras, "3d collision detection: a survey," *Computers & Graphics*, vol. 25, no. 2, pp. 269–285, 2001.

[8] S. Haddadin, A. Albu-Schaffer, A. De Luca, and G. Hirzinger, "Collision detection and reaction: A contribution to safe physical human-robot interaction," in *Intelligent Robots and Systems, IEEE/RSJ International Conference on*, 2008.

[9] H. Taubig, B. Bauml, and U. Frese, "Real-time swept volume and distance computation for self collision detection," in *Intelligent Robots and Systems (IROS), 2011 IEEE/RSJ International Conference on*, 2011.

[10] *IEC EN 60204 2006 - "Safety of machinery. Electrical equipment of machines – General requirements"*.

[11] *ISO 10218 2011 - Robots for industrial environments – Safety requirements – Part 1: Robot*.

[12] *ISO 15066 2013 Robots and robotic devices – Safety requirements for industrial robots – Collaborative operation*.

[13] J. Marvel, "Performance metrics of speed and separation monitoring in shared workspaces," *Automation Science and Engineering, IEEE Transactions on*, vol. 10, no. 2, pp. 405–414, 2013.

[14] A. M. Zanchettin and P. Rocco, "Path-consistent safety in mixed human-robot collaborative manufacturing environments," in *Intelligent Robots and Systems (IROS), 2013 IEEE/RSJ International Conference on*, 2013.

[15] L. Bascetta, G. Ferretti, P. Rocco, H. Ardo, H. Bruyninckx, E. Demeester, and E. Di Lello, "Towards safe human-robot interaction in robotic cells: An approach based on visual tracking and intention estimation," in *Intelligent Robots and Systems (IROS), 2011 IEEE/RSJ International Conference on*, 2011.

[16] S. Kuhn and D. Henrich, "Fast vision-based minimum distance determination between known and unknown object," in *Intelligent Robots and Systems (IROS), 2007 IEEE/RSJ International Conference on*, 2007.

[17] J. Mainprice and D. Berenson, "Human-robot collaborative manipulation planning using early prediction of human motion," in *Intelligent Robots and Systems (IROS), 2013 IEEE/RSJ International Conference on*, 2013.

[18] T. Dietz and A. Verl, "Simulation of the stopping behavior of industrial robots using a complementarity-based approach," in *Advanced Intelligent Mechatronics (AIM), 2011 IEEE/ASME International Conference on*, 2011.

[19] E. Gilbert, D. Johnson, and S. Keerthi, "A fast procedure for computing the distance between complex objects in three-dimensional space," *Robotics and Automation, IEEE Journal of*, vol. 4, no. 2, pp. 193–203, 1988.

[20] A. M. Zanchettin, P. Rocco, L. Bascetta, I. Symeonidis, and S. Peldschus, "Kinematic analysis and synthesis of the human arm motion during a manipulation task," in *Robotics and Automation (ICRA), 2011 IEEE International Conference on*, 2011.

[21] A. M. Zanchettin, L. Bascetta, and P. Rocco, "Achieving humanlike motion: Resolving redundancy for anthropomorphic industrial manipulators," *Robotics Automation Magazine, IEEE*, vol. 20, no. 4, pp. 131–138, 2013.

[22] J. Lenarcic and A. Umek, "Simple model of human arm reachable workspace," *Systems, Man and Cybernetics, IEEE Transactions on*, vol. 24, no. 8, pp. 1239–1246, 1994.

[23] G. Arechavaleta, J.-P. Laumond, H. Hicheur, and A. Berthoz, "An optimality principle governing human walking," *Robotics, IEEE Transactions on*, vol. 24, no. 1, pp. 5–14, 2008.